https://ntrs.nasa.gov/search.jsp?R=19890000819 2020-03-20T06:02:22+00:00Z

54-46
19890000819
617971
18p.

N89-10190

TDA Progress Report 42-94

April–June 1988

Spain 31-GHz Observations of Sky Brightness Temperatures

B. L. Gary
Microwave Observational Systems Section

A water vapor radiometer was deployed at DSS 63 for 3 months of sky brightness temperature measurements at 31 GHz. An exceedance plot has been derived from this data showing the fraction of time that 31-GHz 30-degree elevation angle brightness temperature exceeds specified values. The 5-percent exceedance statistic occurs at 75 K, compared with 70 K in Australia.

I. Introduction

The Deep Space Network is evaluating the merits of using 31 GHz for future spacecraft communications. One part of the Advanced Systems Program is to conduct observations at DSN sites to derive exceedance plots of 31-GHz sky brightness temperature. JPL's Ground-Based Microwave Applications Group was asked to provide these statistics for Spain using the group's SCAMS Water Vapor Radiometer (WVR). In [1], a background is given for acquiring Ka-band weather statistics; Australian results are given in [2].

The SCAMS WVR was deployed in Spain for observations during March 23 to June 28, 1984. The first 10 days of data were taken at the radiosonde launching site at Barajas, seven miles east of Madrid. The next three months were spent at DSS 63, 29 miles west of Madrid.

The Barajas data were intended for use in extrapolating results for the three months at DSS 63 to radiosonde archive-length time bases. (This part of the analysis has not yet been performed.) Another objective was to determine if there was anything unusual about Spain meteorology that would affect the WVR's ability to convert sky brightness temperatures to vapor content and path delay. No differences were found.

II. Observing Setup

Figure 1 is a photograph of the SCAMS WVR. Figure 2 is a photograph of the WVR as it was deployed at DSS 63. The sensor box is on the roof and is tilted (22 degrees) in order to reduce the amount of water that is on the radome cover during (and after) rain. (DSS-63 personnel installed a blower to further assist in reducing "water on radome" problems, but it was rarely used.)

Figure 3 shows what SCAMS prints out in real time. The WVR was programmed to take 100-second tip curve measurements beginning every 10 minutes. Two printout modes are selectable; one shows a sky map of differences from a tip curve fit (lower part), and the other shows estimated brightness temperatures, vapor and liquid, using instrument physical temperature for deriving radiometer gain (upper part). Columns T1 and T2 show the zenith brightness temperature for 22.2 and 31.4 GHz. These are based on real-time tip curve reductions and are very reliable for clear sky conditions.

III. "Tip Curve" Reduction Method

Figure 4(a) is a plot of 22.2- and 31.4-GHz zenith brightness temperatures for a four-day period in April. The horizontal scale has two-hour markers. The vertical scale covers a range of zero to 110 K. The 31.4-GHz data are as low as 12 K (an all-time low for the 3-month observing period at DSS 63). Every day at 1600 UT, the sun passes through one of the tip curve pointing locations and causes a positive feature in this plot. The sky was clear most of this four-day period. Broken clouds were present on April 16, which accounts for some of the midday higher brightness temperatures.

Figure 4(b) is a plot of brightness temperatures for five days of the following week. Most of these data (as presented in this figure) is unusable because of cloud-produced sky brightness temperature "clumpiness." Tip curve reduction algorithms have not yet been developed for deriving good-quality radiometer gains (which are crucial for producing good-quality zenith brightness temperatures). The brightness temperatures that are "zero pegged" are clearly wrong, and they are caused by rainwater resting on the top of the radome (as will be shown below).

The entire data set from DSS 63 has been reduced by the procedure used in producing Figs. 4(a) and (b). A statistical analysis has also been performed on these data. However, since this reduction procedure has serious shortcomings in representing the rainy periods, these statistical results are a very pessimistic interpretation of the Spain measurements, and they will not be presented in this article. Fortunately, another reduction procedure has been developed which "rescues" the rainy periods.

IV. "Gain From Instrument Temperature" Reduction Method

Figure 4(c) is a re-reduction of the 31-GHz raw data used in creating the previous figure and is based on the assumption that knowledge of the SCAMS instrument physical temperature can be used to predict radiometer gain. By overlaying Figs. 4(b) and 4(c), it can be seen that the "well-behaved" parts of Fig. 4(b) agree with the corresponding parts of Fig. 4(c). This provides confidence in the quality of those parts of Fig. 4(c) corresponding to the "poorly behaved" periods of Fig. 4(b).

V. "Off-Zenith" Reduction Method

The reduction procedure that produced Fig. 4(c) still has shortcomings. According to this figure, the 31-GHz zenith sky brightness temperature exceeds 110 K for a period of 3 hours on April 24. If this were a true sky brightness temperature, we could predict that at an elevation of 30 degrees we would expect to measure a brightness temperature exceeding 220 K for the same three-hour period.

Figure 5 is a plot of brightness temperature at one of the 30-degree elevation angle viewing directions (for the same period covered by the previous figure). The vertical scale is compressed by a factor of two so that the top of the plot is actually 220 K. The label for the vertical scale has not been changed, however. This means that the top of the scale, which is 220 K for 30-degree elevation data, can be read as predicting a 110-K brightness temperature at zenith. This is useful for the purpose of detecting non-sky contributions to the measured zenith brightness temperature. If there were no "water on the radome," for example, the two plots would overlap. (Strictly speaking, this is not true, because the 3-K cosmic background component does not double, and saturation effects reduce the doubling for large zenith brightness temperatures.)

Comparing Figs. 4(c) and 5 reveals that "water on radome" effects must have been present during the April 24 high brightness temperature three-hour period. Whereas the average zenith brightness temperature was 123 K between 0400 and 0500 UT, at 30 degrees of elevation it was not twice 123 K but actually lower than at zenith, being 61 K (which would predict a 34-K zenith value).

Figure 6 is a plot of brightness temperature versus zenith angle for the 1-hour period referred to in the previous paragraph. The solid line fits the measured brightness temperatures. The broken line fits the "zenith-derived" brightness temperature, according to the approximate formula: $T_{\text{zen equiv}} = 3 + (T_{\text{meas}} - 3)/\text{air mass}$. A dotted horizontal line is placed at 32 K to indicate the author's estimate of the zenith sky brightness temperature. This plot can be interpreted to mean that water on the radome contributed a component to brightness temperature represented by the difference between the broken line and the dotted line.

Referring to Fig. 6, the 32-K value for zenith brightness temperature is derived by extrapolating a hand-fitted line (fitted to the "zenith equivalent" data) to a zenith angle of 90 degrees which corresponds to the vertical edges of the radome, where, presumably, no water can remain standing. The lowest objectively determined zenith equivalent brightness temperature comes from the +60-degree zenith angle, and this would be a more conservative value to adopt (i.e., 34 K). The minimum zenith equivalent brightness temperature, wherever it occurs, would serve for determining an inferred sky component. This is the procedure that has been adopted for all subsequent data reduction that is described in this article.

Another example of the "off-zenith" method for reducing data is shown in Figs. 7(a) and 7(b). Figure 7(a) is a plot of the tip-curve-based 22- and 31-GHz brightness temperatures, showing that the sky was very "lumpy" for week number 6. Figure 7(b) is a plot of 31-GHz zenith brightness temperature based on radiometer gains that are determined from the instrument physical temperature. It contains both the "sky" and "water on radome" components. Figure 8, in addition to repeating the plot in the previous figure, shows the zenith equivalent brightness temperature derived from the -46- and -60-degree angles. The importance of using the "off-zenith" reduction method is most apparent during two 8-hour periods, one on May 2 and the other on May 3.

Figure 9 is very similar to Fig. 8, except that two-hour averages for the off-zenith data are used. The two-hour average data are obtained automatically by a program that accepts (from the user) gain adjustment information for the week in question, calculates two-hour average zenith-equivalent brightness temperatures for all zenith angles (for each two-hour period), and determines which viewing location was "driest," i.e., had the lowest persistent zenith-equivalent brightness temperature.

In using this automatic procedure for locating the "driest" part of the radome, it is implicitly assumed that any clear areas in the sky do not "hover" over a preferred viewing direction for periods as long as two hours. Indeed, the viewing direction which is found to be "driest" tends to persist for several two-hour periods, implying that the reduction algorithm is actually finding the part of the radome with the least amount of standing water, as opposed to a viewing direction which happened to have the least amount of cloud emission. Therefore, the lowest trace in Fig. 9 appears to be a fair upper-limit estimate of zenith brightness temperature.

Figure 10 is a printout produced by the automatic reducing program described in the previous paragraphs. It is a tabulation of data for week number 1. The dG column is a gain adjustment which the user entered, and will be described later. The right-most columns are average and maximum zenith-equivalent brightness temperatures for each of the five zenith angles. The column labeled "Best" is a duplicate of one entry of one of the five zenith angle columns. For example, the first row is for a two-hour period beginning March 29 at 10 hours UT, and the best viewing direction was +60 degrees. The next row shows a best viewing direction at -60 degrees.

Figure 11 is similar to the plot in Fig. 6, except that it is a plot of the "water on radome" component of measured sky brightness temperature for week number 5. The upper trace indicates maximum amount, and the other traces indicate 75th, 50th, and 25th percentiles. This plot is obtained by blending individual two-hour traces with the zero level established by assuming that the driest viewing direction corresponds to "no water on radome."

Figure 12 is the same kind of plot for week number 6. The maximum "water on radome" effect is displaced toward the west. Presumably, the rain came from the west during this week.

It was mentioned earlier that the user had to enter information about gain adjustments for each particular week. This is accomplished by a three-step procedure. First, a plot of "tip curve derived zenith brightness temperature" is produced. Second, a plot of "instrument physical temperature-based zenith brightness temperature" is produced using the nominal "gain versus temperature" relation (unpublished). This plot can be for any desired offset in anticipation of an overall week's best offset. Third, the two plots are overlaid, and differences during the "well-behaved" parts of the tip curve data are noted. These differences are used to derive a table of gain adjustment values. For example, if the "gain from temperature" plot of zenith brightness temperatures is 1 K too high (compared to the tip curve temperatures), the gain needs to be adjusted by -1.5 units (where a unit is 0.01 count per degree of brightness temperature). This is a labor-intensive procedure and does not lend itself easily to automation. It has been done for all the Spain data. The success of the entire analysis described in this article depends on hand analysis derivations of gain adjustment tables.

Table 1 summarizes the results of the preceding reduction procedure for the entire 14-week observing period at DSS 63. The numbers on the left margin represent "zenith brightness temperature." These values include the components of brightness temperature attributable to the 2.9-K cosmic background, oxygen, water vapor, and liquid water. These results demonstrate that "water on radome" effects have been reduced to a negligible level through use of the elaborate reduction procedure described above.

The numbers in the body of the figure represent the number of occasions having average zenith brightness temperatures of the value indicated on the left, for the week number indicated at the top of the figure. The first column outside the box, on the right, is a summation across all weeks. The next column is a summation of the previous column, summing upward. It is an exceedance tabulation. The last column on the right is the same exceedance tabulation after conversion to percentages. It is to be read in the following manner: X percent of the time, two-hour averages of zenith brightness temperature are equal to, or less than, the brightness temperature value found at the left side of the figure. Thus, 53.5 percent of the time the two-hour averages of zenith brightness

temperature are equal to, or less than, 18 K. (Or, 53.3 percent of the time the two-hour averages of 31-GHz zenith brightness temperature are less than 19 K.)

VI. Results

Figure 13(a) summarizes the statistics on measured sky brightness temperatures for the 14-week observation period at DSS 63. This figure is an exceedance plot. The following example illustrates how this figure should be read: 75 percent of the two-hour averages of measured 31-GHz brightness temperatures correspond to brightness temperatures at a 30-degree elevation angle that are less than 37 K (after excluding the 2.9-K cosmic background component).

Another way to read Fig. 13(a) is illustrated by the following (different) example: 5 percent of the time, two-hour averages of 30-degree elevation angle brightness temperatures exceed 75 K. This brightness temperature level corresponds to an attenuation of about 0.8 dB.

Figure 13(b) is a plot similar to the previous one except that the averaging period is one hour (instead of two hours). The 75-K level is exceeded 5 percent of the time (which is the same as that for the two-hour averaging interval). Table 2 is a tabulation of the one-hour averaging period data.

Figure 14 combines exceedance information contained in the previous two exceedance plots and presents it in a slightly different format. Exceedance plots are shown for the 1-hour and 2-hour data for the high brightness temperatures (the plots are identical for lower brightness temperatures). This figure is to be read: 100-K brightness temperatures (at a 30-degree elevation angle) are exceeded 2.0 percent of the time for the two-hour averaged data and are exceeded 2.3 percent of the time for the one-hour averaged data.

It is not straightforward to produce similar exceedance plots for time intervals that are shorter than one hour. This is due to limitations of the complex reduction procedure used to remove "water on radome" effects. A great amount of time would be involved in extracting this information from the data, and at this time there are no plans to do this.

Figure 16 is an estimate of the family of curves relating exceedance plots to averaging period. The 1- and 2-hour plots are the measured plots from Fig. 14, while the other plot is the author's estimated extrapolation of the data as the observation time interval becomes increasingly small, or "instantaneous."

VII. Rainfall Adjustments

Figure 15 is a plot of rainfall versus season for Barajas. During the 1984 SCAMS observation period, the accumulated rainfall was 15.7 cm instead of the long-term average value of 10.7 cm. The observation period was therefore "wetter" than average. Thus, the exceedance plots presented in this article correspond to "wetter than average" conditions.

Rain-related weather defines the location and shape of the high brightness temperature end of the exceedance plots. There was 47 percent more rain during the observation period than during a typical April through June period. There must be many ways of adjusting the exceedance plots to produce a plot that corresponds to different weather conditions. The straightforward and intuitive assumption is that the "height" of the exceedance plot (at the high brightness temperature end) is directly proportional to the rate of rainfall for the interval in question. This method was used to produce Fig. 16, which is perhaps the best estimate that can be made from the SCAMS measurements of exceedance plots for average weather at DSS 63. This figure is the final product of this report.

Acknowledgment

The author wishes to thank Robert Clauss for suggesting that equivalent zenith brightness temperatures can be derived from off-zenith measurements, as described in Section V.

References

[1] S. D. Slobin, "Models of Weather Effects on Noise Temperature and Attenuation for Ka- and X-Band Telemetry Performance Analysis," *TDA Progress Report 42-88*, vol. October–December 1986, Jet Propulsion Laboratory, Pasadena, California, pp. 135–140, February 15, 1987.

[2] B. L. Gary, "Australia 31-GHz Observations of Sky Brightness Temperatures," *TDA Progress Report 42-94*, vol. April–June 1988, Jet Propulsion Laboratory, Pasadena, California, August 15, 1988.

Table 1. Statistical summary of Spain data after correction for radome water effects: 2-hour averages

Zenith brightness temperature, K	Week number[a]														Exceedance statistics		
	1	2	3	4	5	6	7	8	9	10	11	12	13	14	Σ	ΣΣ	%
>80			1		2	–	–	–		–	1	2	–		6	994	100.0
61–80			–		2	–	2	2		3	–	1	2		12	988	99.4
51–60			5		2	–	6	3		1	–	–	–		17	976	98.2
41–50	3		7		1	3	1	7		2	3	2	1		30	959	96.5
31–40	6	2	6		3	7	7	8	7	12	3	1	4		66	929	93.5
26–30	4	2	7		3	3	4	13	7	3	3	3	6	1	59	863	86.8
23–25	11	–	2		5	2	6	8	3	6	9	2	6	2	62	804	81.0
21–22	4	–	2		4	2	4	5	5	3	5	5	27	15	81	742	74.7
20	5	3	2	1	–	2	4	4	6	2	7	3	17	5	61	661	66.6
19	4	–	4		5	3	2	4	6	6	12	4	15	4	69	600	60.4
18	2	4	5		6	4	2	9	7	3	15	20	7	8	92	531	53.5
17	2	8	31	1	7	3	–	9	5	11	13	10		1	101	439	44.2
16	1	26	6	10	10	1	8	12	16	14	2	9		2	117	338	34.0
15	2	20		15	28	4	14	6	8	15	7	17			136	221	22.3
14	2	6		15	–	1	16	3	2	2	2	4			53	85	8.6
13				10	5	2	4	1							22	32	3.2
12				6			1	3							10	10	1.0
Totals	46	71	78	58	83	37	81	97	72	83	82	83	85	38	994		

[a]Data show the number of occations that 2-hour averages had the corresponding sky zenith brightness temperature.

Table 2. Statistical summary of Spain data with hourly averages

Zenith brightness temperature, K[b]	Week number[a]														Exceedance statistics		
	1	2	3	4	5	6	7	8	9	10	11	12	13	14	Σ	ΣΣ	%
>80	–	–	1		3		1	3		3	1	4	–		16	1982	100.0
61–80	–	–	4		4		2	4		4	1	2	4		25	1966	99.2
51–60	1	–	9		2	1	10	5		2	2	2	–		34	1941	97.9
41–50	6	2	7		1	6	6	10	2	5	2	2	2		51	1907	96.2
31–40	9	–	16		7	15	11	21	12	13	10	3	5	1	123	1856	93.6
26–30	12	2	11		10	6	10	18	7	13	2	2	16	–	109	1733	87.4
23–25	12	1	6		14	5	6	10	9	12	12	9	13	1	110	1624	81.9
21–22	11	3	2		11	8	5	13	11	5	17	10	25	11	132	1514	76.4
20	8	2	2	2	9	6	4	6	11	5	14	4	42	16	131	1382	69.7
19	11	–	4	–	21	9	–	13	16	9	21	6	45	11	166	1251	63.1
18	7	6	9	–	27	5	2	18	13	11	34	39	13	14	198	1085	54.7
17	5	6	51	2	38	2	12	18	17	20	29	21	3	15	240	887	44.8
16	–	31	20	20	14	1	10	30	18	30	5	15		6	200	647	32.6
15	3	55	3	30	3	5	22	18	17	31	9	30		1	227	447	22.6
14	5	27		30		3	33	3	4	3	4	12		2	126	220	11.1
13	2	4		20			22	2	5	1	1	6			63	94	4.7
12	–	2		12			8		3		5	1			31	31	1.6
Totals	92	141	145	116	164	73	164	192	145	167	169	168	168	78	1982		

[a]Data show the number of occations that 2-hour averages had the corresponding sky zenith brightness temperature.

[b]Includes 2.9 K.

ORIGINAL PAGE IS
OF POOR QUALITY

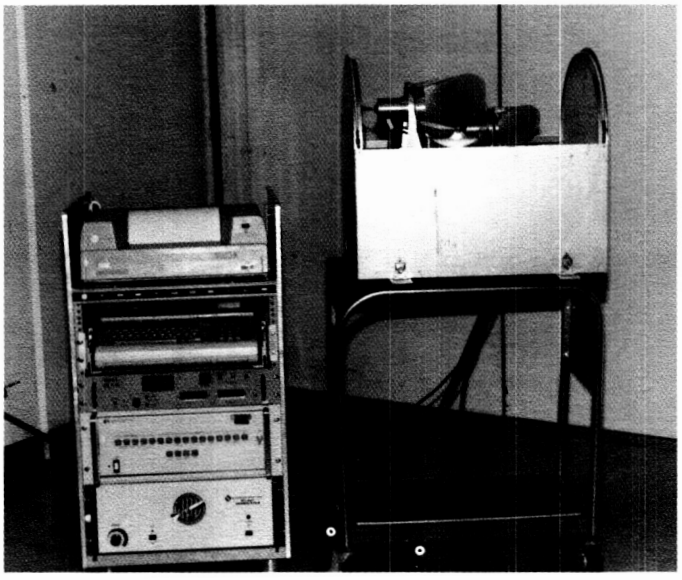

Fig. 1. Photograph of the SCAMS water vapor radiometer system prior to deployment

Fig. 2. Photograph of the SCAMS after deployment on the roof of the main control building at DSS 63. The view is to the south.

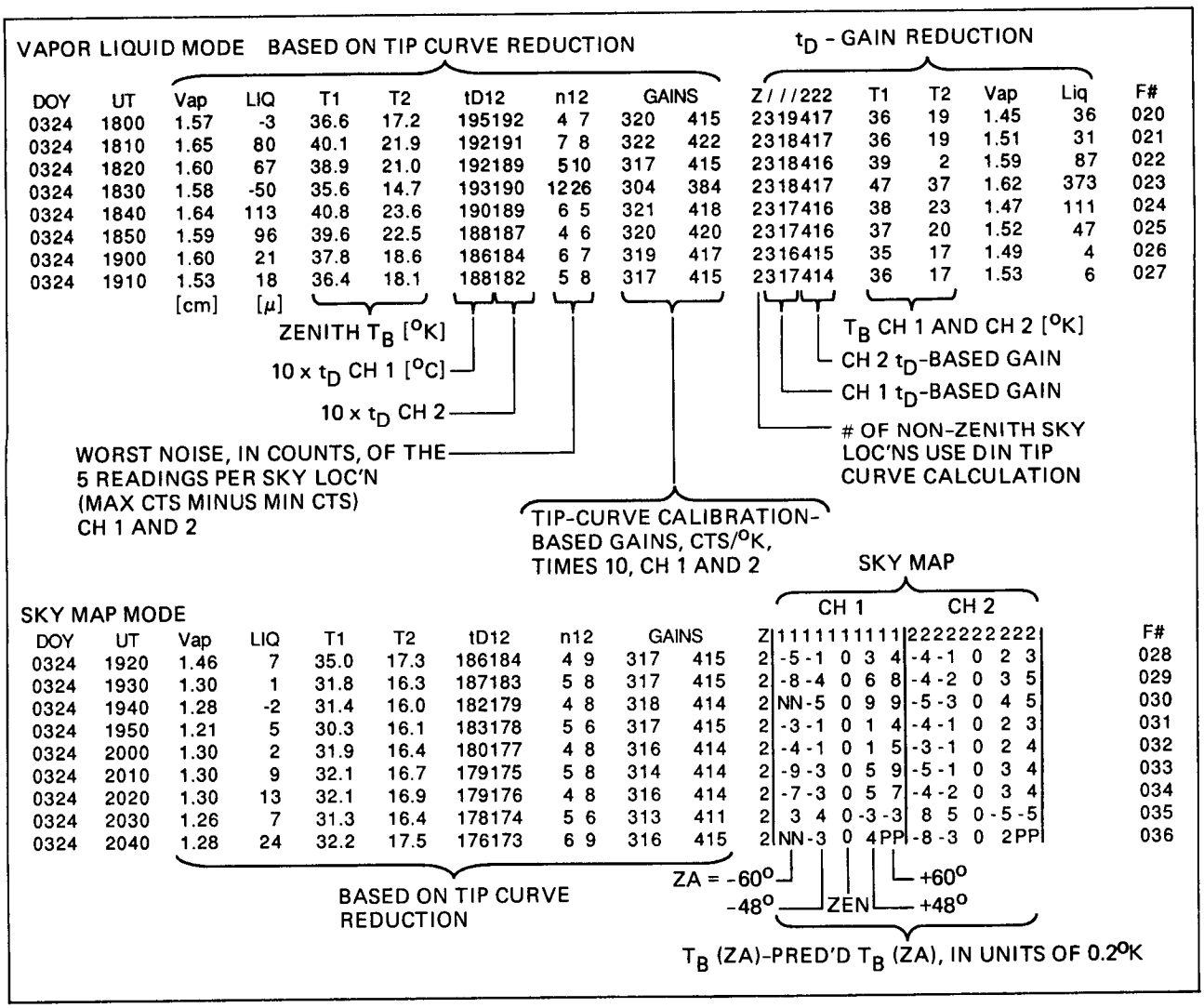

Fig. 3. Real-time printouts of the SCAMS observing program. Printouts for two data reduction modes are displayed.

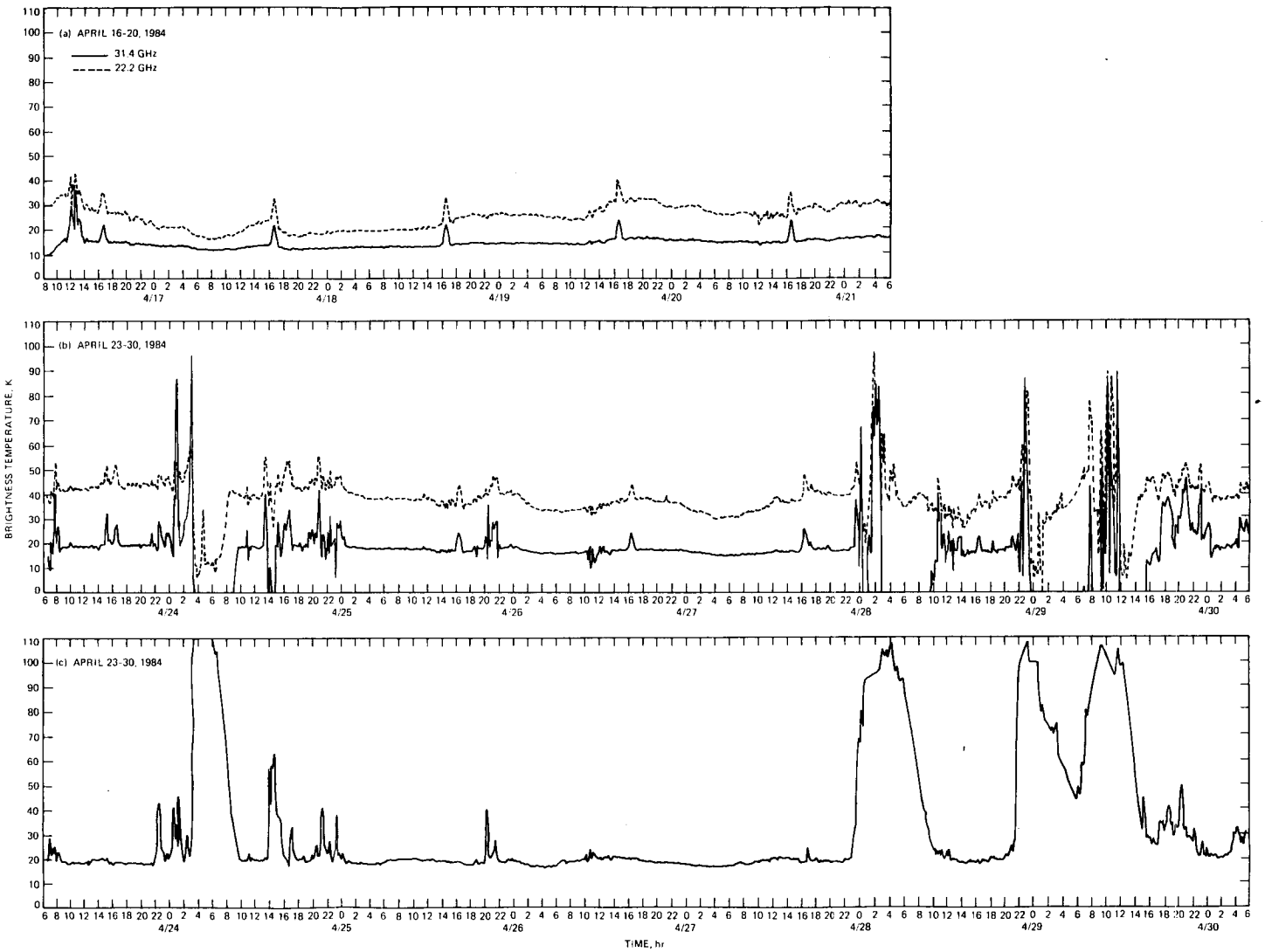

Fig. 4. Brightness temperatures for various dates and conditions at DSS 63: (a) plot of 22.2- and 31.4-GHz zenith brightness temperatures from April 16–21, 1984; (b) plot of brightness temperatures during cloudy conditions from April 23–30, 1984; (c) plot of the 31.4-GHz brightness temperature for the same period as shown in (b), using a data reduction algorithm that should give better results for cloudy conditions by deriving instrument gain from a gain versus instrument temperature relation, rather than deriving gain from tip curves.

FOLDOUT FRAME

FOLDOUT FRAME

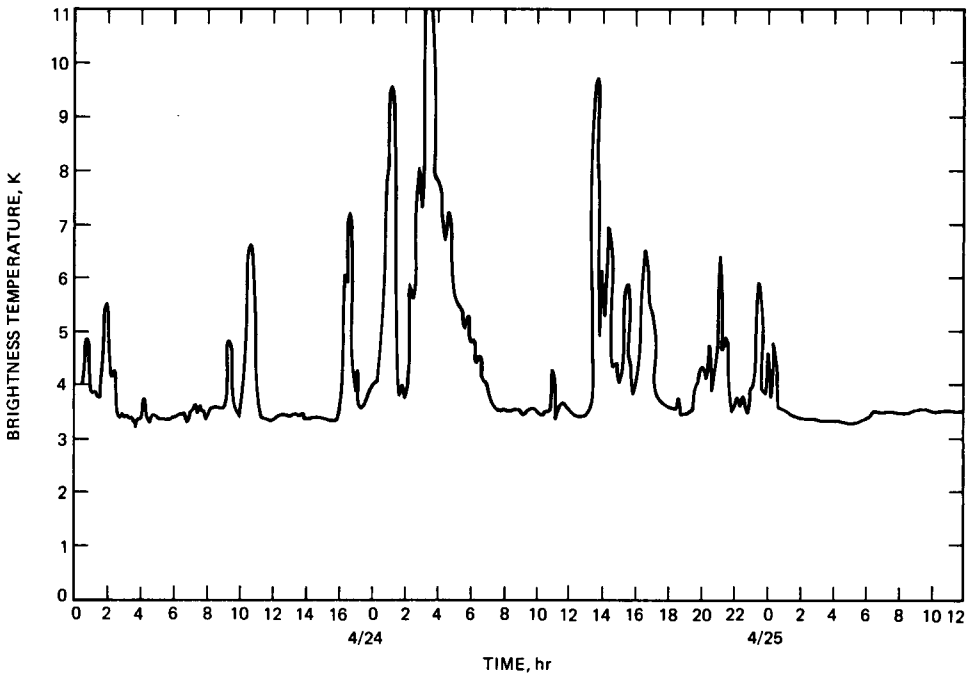

Fig. 5. The 31.4-GHz brightness temperatures for the viewing direction +60 zenith angle for the same period as Fig. 4(c). The Y-axis scale, shown extending from 0 to 110 K, is actually for 0 to 220 K. If the trace is thought of as a zenith equivalent brightness temperature, then the scale 0 to 110 K is appropriate.

PRECEDING PAGE BLANK NOT FILMED

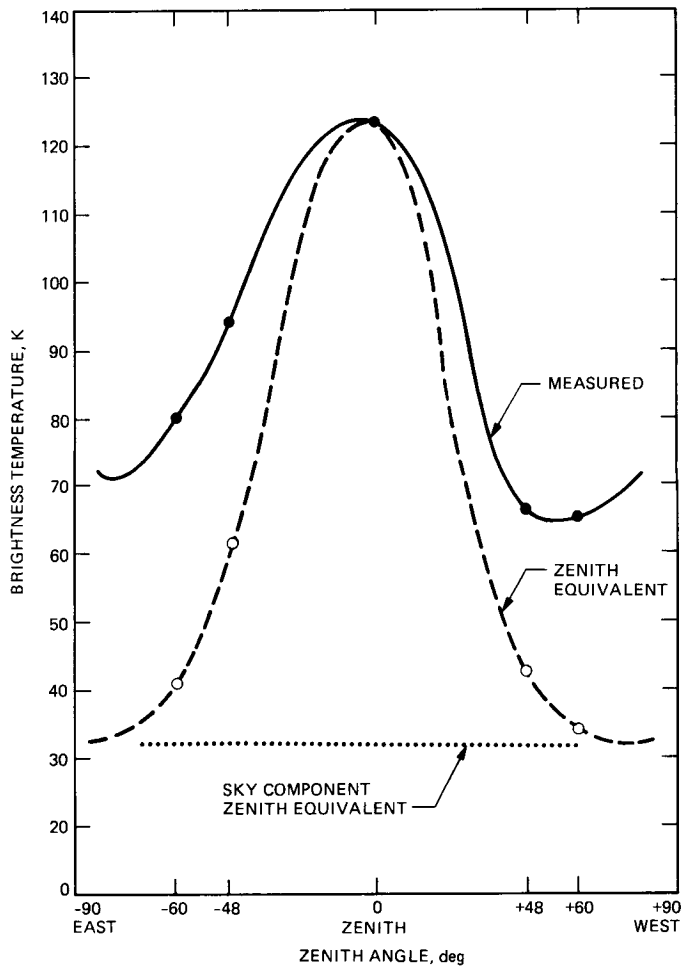

Fig. 6. Comparison of 31.4-GHz brightness temperatures at various zenith angles during a 1-hour period in which water is suspected of being on the radome. The dashed line is the zenith equivalent brightness temperature and the horizontal dotted line is the "no water" component attributable to the sky.

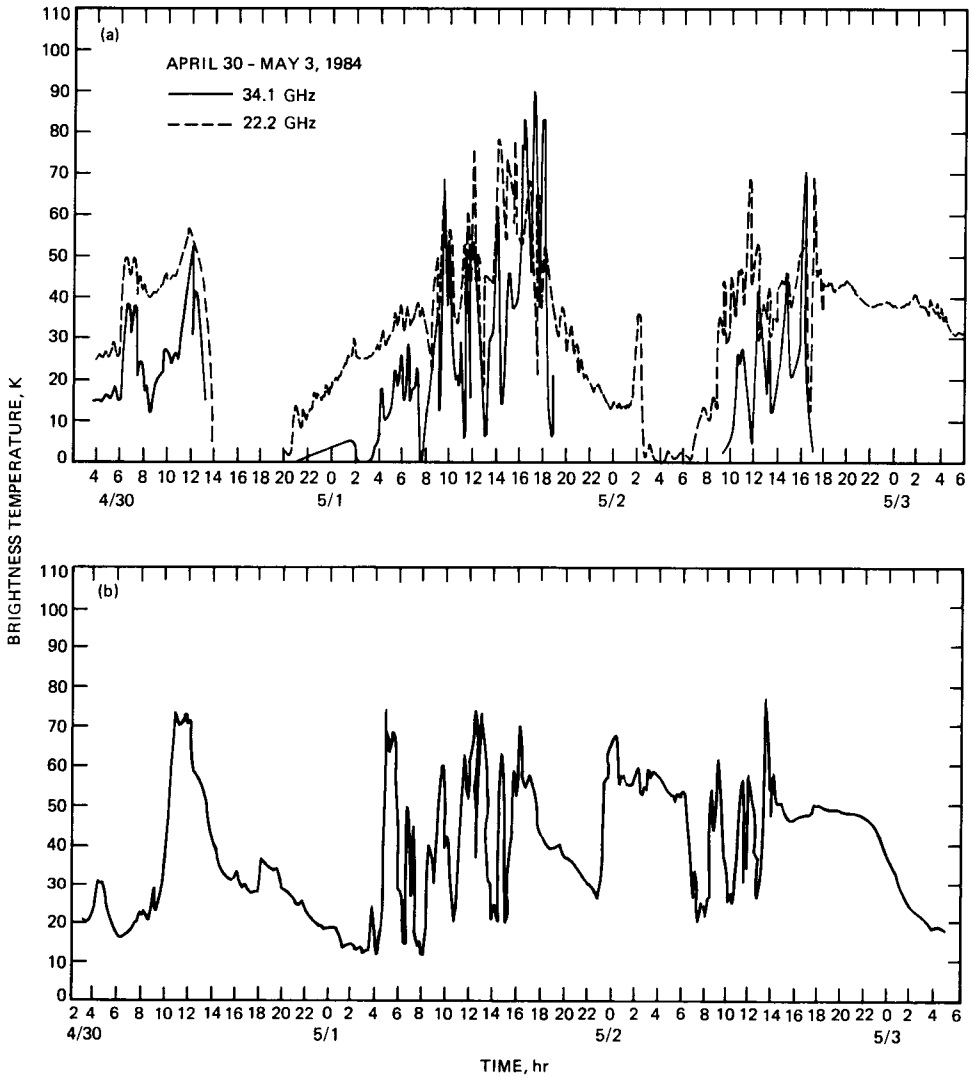

Fig. 7. Brightness temperatures for a second period during which water is suspected of being on the radome: (a) 22.2- and 31.4-GHz plot based on tip curve; (b) plot of zenith brightness temperatures based on the "instrument gain versus instrument physical temperature" relationship. Note that (b) is better behaved than (a).

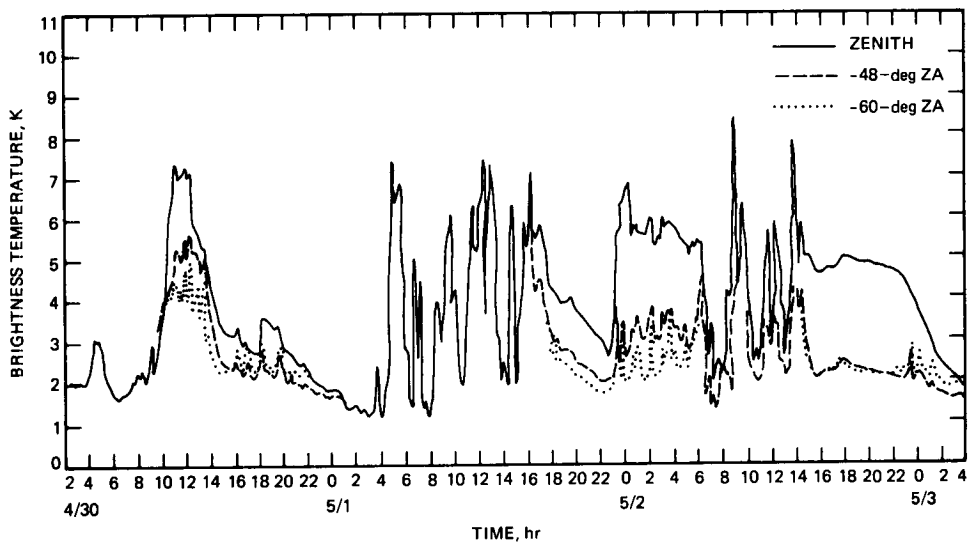

Fig. 8. Plot of zenith equivalent 31.4-GHz brightness temperatures derived from the observed brightness temperatures at 0, −48, and −60 degrees zenith angle. The observed zenith angle = 0 brightness temperature trace is taken from the previous figure.

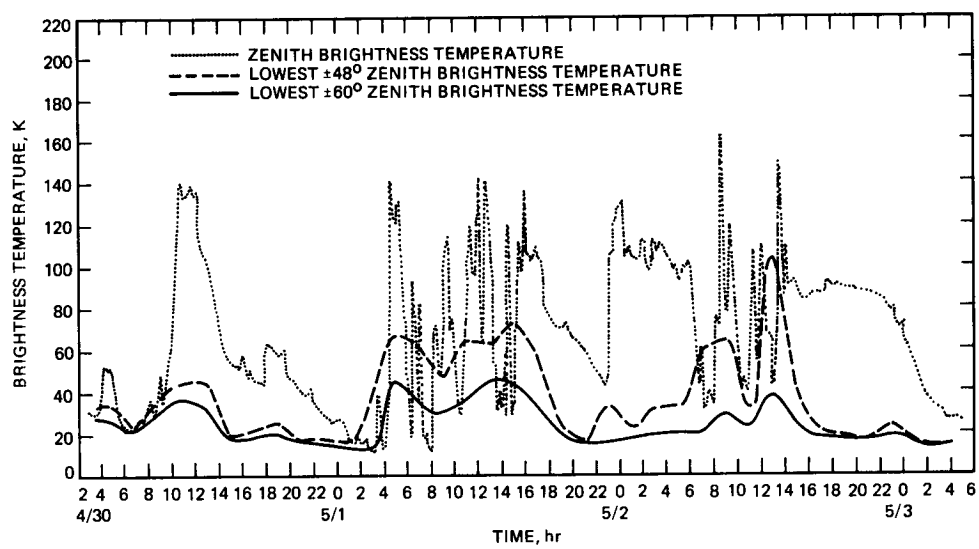

Fig. 9. The dotted line trace, taken from the previous figure, represents the zenith brightness temperature. The two bottom traces represent the lowest measured brightness temperatures during 2-hour observation periods at ±48 and ±60 zenith.

DATE/UT	dG	BEST		-60		-48		ZEN		+48		+60	
32910	4	23	30	23	29	25	32	28	40	25	32	23	30
32912	3	24	34	24	34	26	34	29	34	27	35	25	32
32914	2	31	57	31	57	36	70	60	109	46	74	39	61
32916	2	41	45	41	45	53	61	80	90	51	73	43	60
32918	1	41	62	41	62	46	68	95	114	62	87	51	68
32920	0	43	55	43	55	49	58	89	129	61	70	51	61
32922	-0	30	42	30	42	40	54	47	71	45	63	34	48
33000	-1	27	36	27	36	34	47	54	85	38	58	31	45
33002	-2	23	26	23	26	24	26	41	46	30	37	23	26
33004	-2	20	21	21	23	22	23	32	37	23	26	20	21
33006	-3	23	34	23	34	25	31	26	30	27	51	24	29
33009	-4	21	23	21	23	22	25	25	30	23	27	24	37
33012	-5	21	23	21	23	22	24	29	55	33	96	25	29
33015	-6	24	30	24	30	24	32	26	38	30	52	26	32
33017	-6	32	58	32	58	41	76	67	165	48	132	44	103
33019	-7	25	37	25	37	27	37	33	56	26	39	26	57
33021	-8	20	20	21	22	21	23	23	24	20	21	20	20
33023	-8	18	18	19	20	19	20	20	22	18	19	18	18
33100	-8	18	19	19	21	19	19	19	20	18	19	18	19
33102	-7	19	21	20	26	21	27	21	27	19	22	19	21
33104	-7	19	20	22	26	23	27	21	25	20	22	19	20
33106	-6	16	23	18	27	17	26	16	23	16	21	16	19
33108	-6	14	22	16	18	16	18	14	22	15	19	16	21
33110	-5	32	38	32	38	34	42	36	54	41	56	42	57
33112	-5	37	82	44	83	51	82	37	82	41	73	38	59
33114	-4	34	68	34	68	39	84	59	122	62	111	55	94
33116	-4	23	33	23	33	23	37	26	51	32	56	34	52
33118	-3	38	97	40	104	47	113	68	152	43	106	38	97
33120	-3	21	51	21	51	22	66	43	98	25	70	22	57
33122	-3	15	17	15	17	15	19	19	25	21	36	21	37
40100	-2	17	29	17	29	19	34	22	58	20	37	18	29
40102	-2	15	22	15	21	15	22	15	21	16	22	16	21
40104	-1	26	51	26	51	31	61	43	92	36	55	34	50
40106	-1	17	20	18	21	17	20	18	29	18	23	18	21
40108	-0	20	24	20	24	20	27	23	29	25	33	26	34
40110	0	28	41	28	41	30	42	36	46	37	47	34	44
40112	1	21	28	21	28	22	28	27	37	33	56	33	53
40114	1	23	26	23	26	26	31	30	37	38	50	32	45
40116	2	23	30	23	30	24	30	25	31	26	44	24	35
40118	2	24	28	26	35	24	28	25	29	25	33	24	29
40120	3	24	29	26	35	25	33	26	30	25	32	24	29
40122	3	20	20	20	20	20	21	21	22	20	21	20	20
40200	3	19	20	20	20	20	20	19	20	19	20	19	20
40202	3	19	21	19	20	20	22	20	24	19	22	19	21
40204	3	20	22	20	22	21	23	22	26	22	28	24	29

Fig. 10. Output of a program that automatically performs the "off-zenith" correction for water-on-radome effects

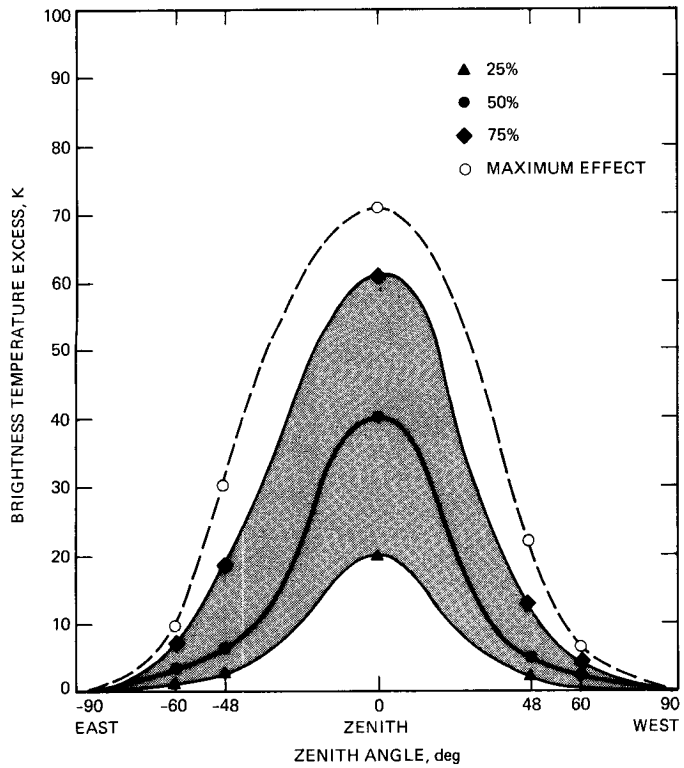

Fig. 11. Statistics for a week of data that are presumably affected by water on the radome, showing the component of 31.4-GHz brightness temperature versus zenith angle due to water on the radome. Percentile lines are shown for 25, 50, and 75 percent. A maximum effect trace is shown with a broken line.

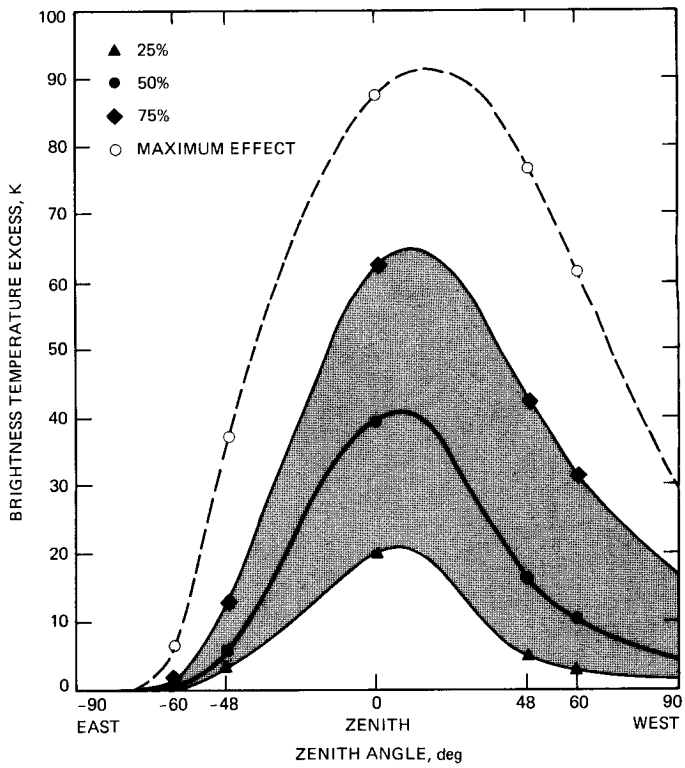

Fig. 12. Statistics analogous to those of Fig. 11 for a different week of data

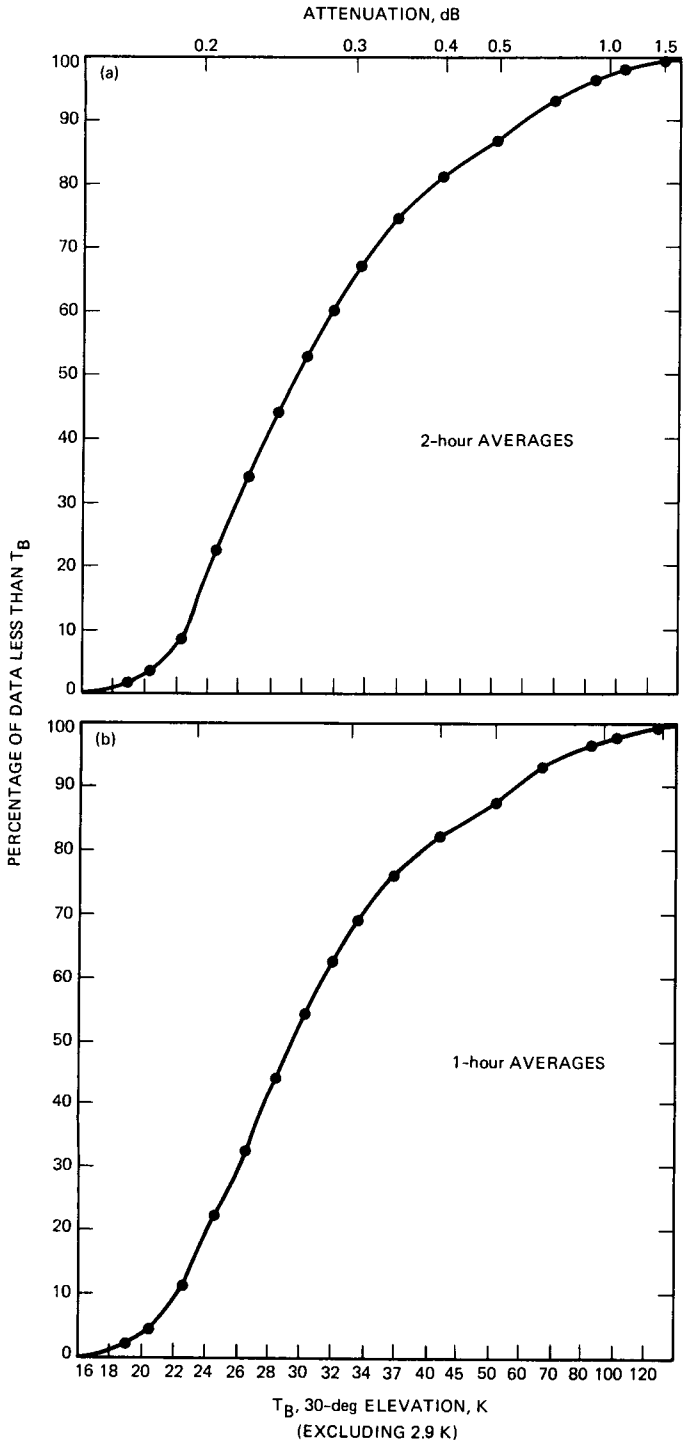

Fig. 13. Exceedance plots for 31.4-GHz sky brightness temperature for an elevation angle of 30 degrees: (a) data from 2-hour averages used; (b) data from 1-hour averages used.

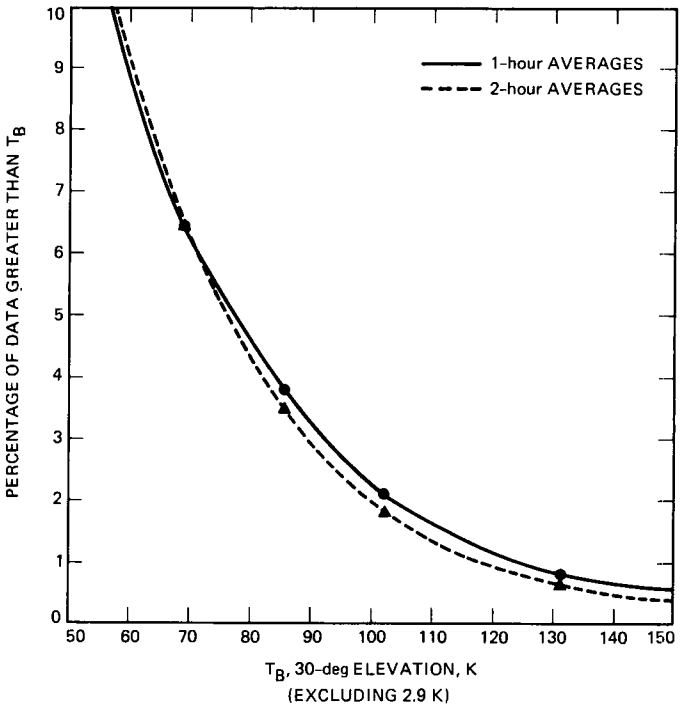

Fig. 14. Exceedance plots of 1- and 2-hour data averages for the "high end." The Y-axis is the percent of time that 30-degree elevation angle 31.4-GHz sky brightness temperature exceeds the X-axis value.

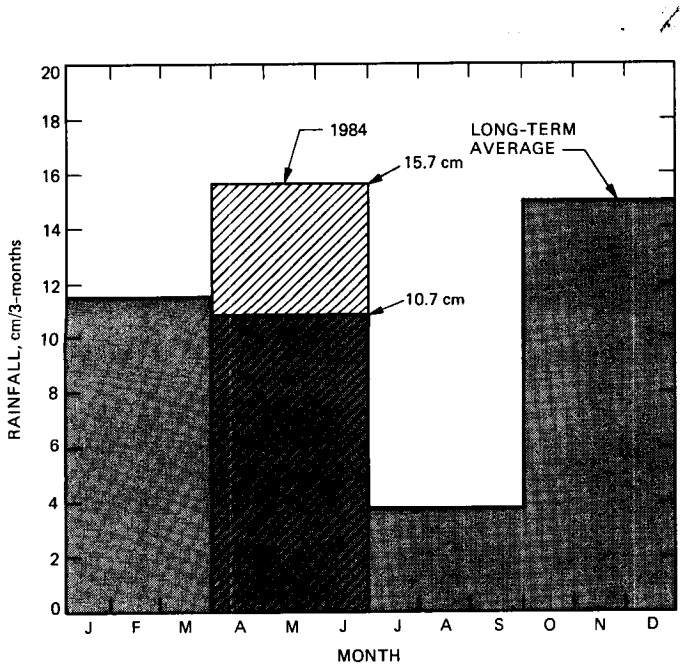

Fig. 15. Rainfall statistics for the 3-month observation period compared with historical averages. The observing period had 47 percent more rain than typical.

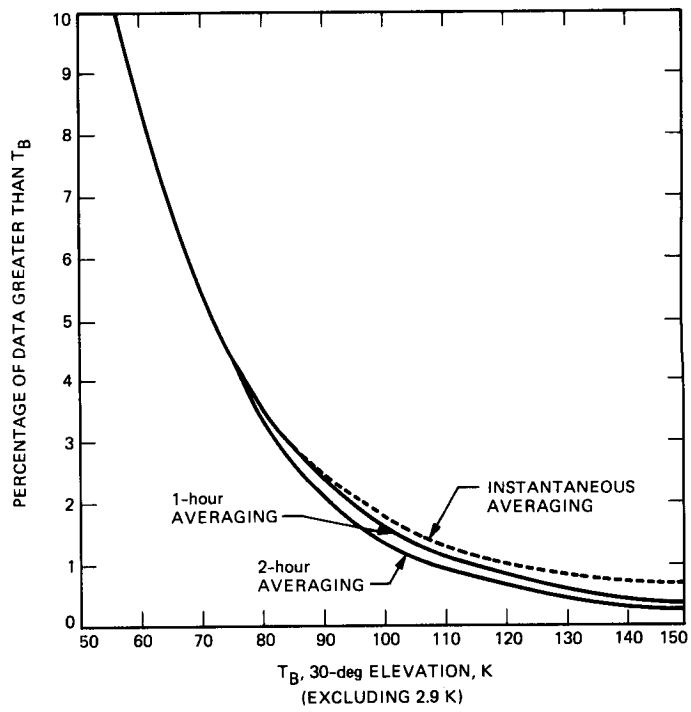

Fig. 16. Final plot of 31.4-GHz 30-degree elevation angle sky brightness temperature exceedances. The plots reflect a correction for the greater than average rainfall that occurred during the 14-week observation period. The 1- and 2-hour data averages are based on real data, whereas the broken line is an estimate for "instantaneous" statistics.